Available online at www.sciencedirect.com
ScienceDirect
Inorganica Chimica Acta 361 (2008) 769–777
Inorganica Chimica Acta
www.elsevier.com/locate/ica

Binding and direct electrochemistry of OmcA, an outer-membrane cytochrome from an iron reducing bacterium, with oxide electrodes: A candidate biofuel cell system

Carrick M. Eggleston [a,*], Janos Vörös [b], Liang Shi [c], Brian H. Lower [d], Timothy C. Droubay [e], Patricia J.S. Colberg [f]

[a] *Department of Geology and Geophysics, University of Wyoming, Laramie, WY 82071, United States*
[b] *Institute for Biomedical Engineering, Swiss Federal Institute of Technology, Gloriastrasse 35, CH-8092 Zürich, Switzerland*
[c] *Division of Biological Sciences, Pacific Northwest National Laboratory, Richland, WA 99352, United States*
[d] *Environmental Molecular Science Laboratory, Pacific Northwest National Laboratory, Richland, WA 99352, United States*
[e] *Fundamental Science Directorate, Pacific Northwest National Laboratory, Richland, WA 99352, United States*
[f] *Department of Zoology and Physiology, University of Wyoming, Laramie, WY 82071, United States*

Received 5 March 2007; received in revised form 11 July 2007; accepted 25 July 2007
Available online 3 August 2007

Dedicated to Professor Michael Grätzel

Abstract

Dissimilatory iron-reducing bacteria transfer electrons to solid ferric respiratory electron acceptors. Outer-membrane cytochromes expressed by these organisms are of interest in both microbial fuel cells and biofuel cells. We use optical waveguide lightmode spectroscopy (OWLS) to show that OmcA, an 85 kDa decaheme outer-membrane *c*-type cytochrome from *Shewanella oneidensis* MR-1, adsorbs to isostructural Al_2O_3 and Fe_2O_3 in similar amounts. Adsorption is ionic-strength and pH dependent (peak adsorption at pH 6.5–7.0). The thickness of the OmcA layer on Al_2O_3 at pH 7.0 [5.8 ± 1.1 (2σ) nm] from OWLS is similar, within error, to that observed using atomic force microscopy (4.8 ± 2 nm). The highest adsorption density observed was 334 ng cm^{-2} (2.4×10^{12} molecules cm^{-2}), corresponding to a monolayer of 9.9 nm diameter spheres or submonolayer coverage by smaller molecules. Direct electrochemistry of OmcA on Fe_2O_3 electrodes was observed using cyclic voltammetry, with cathodic peak potentials of −380 to −320 mV versus Ag/AgCl. Variations in the cathodic peak positions are speculatively attributed to redox-linked conformation change or changes in molecular orientation. OmcA can exchange electrons with ITO electrodes at higher current densities than with Fe_2O_3. Overall, OmcA can bind to and exchange electrons with several oxides, and thus its utility in fuel cells is not restricted to Fe_2O_3.

Keywords: Cytochrome; OmcA; Adsorption; Voltammetry; OWLS; AFM

1. Introduction

The discovery of dissimilatory iron-reducing bacteria (DIRB) has had a far-reaching impact on our understanding of the global biogeochemical cycling of Fe, Mn, associated trace elements and phosphate, on the degradation of organic matter, and on the weathering of ferric minerals. Bacterial Fe(III) reduction is believed to be one of the earliest respiratory processes to have evolved [1,2] and is the second most common respiratory process after oxygen reduction [3,4]. There are a number of bacteria from a wide variety of habitats that are now known to couple reduction of Fe(III) and other metals to the oxidation of organic matter [5–13].

Unlike the freely soluble electron acceptors most often used by other prokaryotes, DIRB transfer their electrons to solid minerals, commonly Fe(III) or Mn(IV) oxyhydrox-

* Corresponding author. Tel.: +1 307 766 6769; fax: +1 307 766 6679.
E-mail address: carrick@uwyo.edu (C.M. Eggleston).

0020-1693/$ - see front matter © 2007 Elsevier B.V. All rights reserved.
doi:10.1016/j.ica.2007.07.015

ides [3,7,14]. They have evolved several strategies for utilization of such low solubility terminal electron acceptors; these include shuttling electrons from their electron transport chain to mineral surfaces via humic acids [15] or by producing electrically conducting pili, so-called bacterial 'nanowires' [16,17]. DIRB genomes also encode for an unusually large number of *c*-type cytochromes [18,19] (membrane-bound, heme-containing proteins best known for their role in electron transport). Some of these are known to be expressed on the outer surface of the outer-membrane [20–23] and so may act as terminal reductases for electron transfer to mineral surfaces [24–27].

Microbial fuel cells (MFC) are devices that use bacteria to oxidize organic substrates and generate current [28,29]. Electrons produced from the substrates are transferred to an anode and flow through a conductor to a cathode through a resistive load. Electrons can be transferred to the anode by electron shuttle compounds, by nanowires, or by membrane-associated proteins. In related biofuel cells, enzymes immobilized on electrode surfaces catalyze oxidation of fuels and transfer electrons to an electrode [27]. The outer-membrane *c*-type decaheme cytochrome OmcA, from the DIRB *Shewanella oneidensis* MR-1, appears to possess many of the characteristics needed to develop such biofuel cells and would likely play a role in *Shewanella*-based MFCs. Xiong et al. [27] recently demonstrated that OmcA binds to, and can be oxidized by, hematite (Fe_2O_3) nanoparticles at pH 7. They claim further that OmcA adsorption to hematite is specific and that OmcA does not bind strongly to other minerals like goethite (FeOOH) and diaspore (AlOOH).

The diversity of electrode materials to which a given protein will bind is important in biofuel cell design. If OmcA binding is specific to Fe_2O_3 but much more limited for other solids, then the potential utility of OmcA in a biofuel cell may be limited because hematite has a relatively low charge carrier mobility [30,31] and may not be an optimum anode material. Other materials (e.g., F-doped SnO_2, graphite) may be preferable.

Here, we show that OmcA adsorbs similarly to Al_2O_3 and Fe_2O_3 (oxides chosen to present one redox-active, and another redox-inactive but otherwise similar, surface to the OmcA) as a function of pH, a result that appears contrary to that of Xiong et al. [27]. We also demonstrate direct electrochemistry between OmcA and both Fe_2O_3 (chosen because it is the only nominal ferric oxide that is sufficiently conductive to use as a working electrode in cyclic voltammetry) and indium–tin oxide (ITO) (chosen because it is a common conductive oxide material that may be of interest in biofuel cell applications) electrodes. We conclude that OmcA may be useful as a direct redox catalyst with a variety of electrode materials. Indeed, hematite has a relatively high-potential conduction band edge compared to the more commonly occurring ferric (hydr)oxides, and it would be surprising if DIRB were not adapted to access the commonly occurring ferric minerals in soils and sediments rather than to hematite in particular.

2. Experimental

2.1. Optical waveguide lightmode spectroscopy (OWLS)

OWLS has been used extensively in the study of protein adsorption/binding to a variety of oxide surfaces [32–37]. The technique relies on measurement of changes in the effective refractive index of an oxide waveguide as a result of adsorption of proteins or other molecules to the waveguide surface. The effective refractive index of the waveguiding film can be used in the waveguide mode equations [38] to extract the refractive index of the adsorbed adlayer material, given that the refractive index of the covering medium (e.g., buffer) is known. This can, in turn, be related to the mass of adsorbed protein by de Feijter's formula,

$$M = d_A\left[\frac{n_A - n_C}{dn/dc}\right]$$

where d_A is the thickness of the adsorbed adlayer, n_A and n_C are the refractive indices of the adlayer and of the covering medium, respectively, and dn/dc is the dependence of refractive index on protein concentration; dn/dc has been determined to be 0.182 cm^3/g for most proteins, including cytochromes [34,36].

We used Al_2O_3-coated (MicroVacuum Ltd., Budapest, Hungary) and Fe_2O_3 coated (made by molecular beam epitaxy at Pacific Northwest National Laboratory, Richland, Washington) $(Ti_{0.75}Si_{0.25})O_2$ waveguides (MicroVacuum Ltd.) in our OWLS measurements. We used OWLS 110 and OWLS 120 instruments (MicroVacuum Ltd.); both models use the same basic measurement apparatus.

For Fe_2O_3 coating, an uncoated $(Ti_{0.75}Si_{0.25})O_2$ waveguide was ultrasonically cleaned in isopropyl alcohol and methanol, mounted on a sample holder, and inserted into ultra-high vacuum. A thin (~0.5 mm) Mo foil was used as a mask to limit Fe_2O_3 deposition to the grating area of the waveguide. Within the deposition chamber, the waveguide was cleaned with atomic oxygen from an electron cyclotron resonance oxygen plasma source at a chamber pressure of $\sim 2\times10^{-5}$ Torr for 5 min to rid it of adventitious carbon. The Fe_2O_3 film was grown in excess atomic oxygen using an Fe metal evaporation rate of ~0.01 nm/s, which has been shown to produce single crystal epitaxial α-Fe_2O_3 on α-$Al_2O_3(0001)$ substrates [39,40]. Atomic absorption, previously calibrated using a quartz crystal microbalance, controls the metal flux during oxide film growth and allows for precise thickness control. Room temperature growth on non-lattice-matched substrates using these deposition conditions results in polycrystalline hematite films. A Fe_2O_3 thickness of ~2 nm was deposited on the waveguide to ensure complete grating coverage without degrading sensitivity. Following growth, the Fe flux from the electron beam evaporator was eliminated using a shutter while the coated waveguide was bathed in atomic oxygen to guarantee complete oxidation.

The Fe_2O_3-coated waveguide was only available on our final day of instrument time, allowing us time for only three measurements. Nevertheless, the results are sufficient for comparison of OmcA adsorption to Fe_2O_3 and Al_2O_3 under similar conditions.

OWLS measurements indicated a waveguide thickness of 167.7 nm prior to coating with Fe_2O_3 and a thickness of 172.6 nm after coating. This discrepancy is consistent with the fact that layer thicknesses from OWLS are generally rather inaccurate and subject to covariance with the layer refractive index measurement.

Before each OWLS measurement, the waveguide was cleaned in oxygen plasma for one min; a baseline reading was established in the OWLS instrument for each waveguide and protein-free buffer. A stable baseline took up to 3 h to achieve, probably because of rehydration of the oxide surface after the plasma cleaning step. With a stable baseline, 100 μL of the OmcA solution (5.3×10^{-7} M, 0.045 mg/mL) was injected into the OWLS fluid cell. After equilibration, protein-free buffer was injected into the fluid cell, and the OWLS signal monitored for desorption. In general, we found that very little protein desorbed upon dilution. Buffer refractive indices were measured to five significant figures using a Leica digital refractometer and were used in the adsorbed-mass calculations (BioSense software, MicroVacuum Ltd.) for each set of conditions.

Only one measurement was made at each pH value due to the availability of only very small amounts of protein and limited instrument time. Subsequent multiple determinations of adsorption density using another protein (5 replicates) gave a reproducibility of ± 3 ng cm^{-2} (2σ).

2.2. OmcA

OmcA (SO1779) is an 85 kDa decaheme outer-membrane *c*-type cytochrome from *S. oneidensis* MR-1. The native protein includes a lipid-binding site that is presumed to hydrophobically anchor the protein to the outer-membrane [42]. In this adsorption study, we are primarily interested in the interaction of the redox active portions of the protein with a mineral surface. Although the structure of OmcA is not yet known, it is reasonable to assume that the lipid-binding site would be attached to the outer-membrane, leaving the portion of the protein suited for interaction with the mineral, roughly speaking, on the opposite side. Because we are not as interested in the interaction of the hydrophobic lipid with the mineral surface as we are in the interaction of other parts of the protein with the mineral surface, we used an OmcA lacking the lipid-binding site in all of our adsorption experiments. OmcA retaining the lipid-binding site was, however, used in the electrochemical experiments because preparations lacking the binding site were not available at the time of these experiments. Subsequent work (data not shown) indicates no significant difference in the redox behavior of the two constructs.

To create an OmcA lacking the lipid-binding site, the coding sequence for signal peptide and the lipid-binding site of OmcA was replaced by the coding sequence for the signal peptide and first two amino acids of MtrB (SO1776), which is not a lipoprotein. The coding sequence for the signal peptide and the first two amino acids of MtrB, and for OmcA without signal peptide and lipid-binding site, were amplified individually. The equal molar amounts of the first round of PCR products were mixed and then used as template for a second round of PCR. The second round of PCR products were gel purified and cloned into a protein expression vector described previously [41]. The resulting plasmid, pLS147, was sequenced to confirm that the coding sequence for signal peptide and the first two amino acids of MtrB and the coding sequence for OmcA without signal peptide and a lipid-binding site were successfully linked before it was used to transform a knock-out mutant of *S. oneidensis* MR-1 that lacks expressed OmcA and MtrC (ΔomcA/mtrC) [42]. OmcA with the lipid-binding site and with a tetracysteine tag was expressed, harvested, and purified as described previously. The results of EPR and metal reductase analysis of purified OmcA demonstrated that deletion of the lipid-binding site of OmcA alters neither its redox properties nor metal reductase activity [41,42].

For OWLS measurements, the tagless OmcA was exchanged into 10 mM KCl (no precipitation was observed), and 30 μL aliquots of this solution were diluted into 70 μL of buffers at different pH values for OWLS measurements with a total sample volume of 100 μL. pH was checked after dilution into buffer at pH 7 and 7.5 and was within 0.1 pH units of the pH of the buffer used for dilution. Buffers were all 10 mM and were all adjusted to the target pH with HCl or NaOH: pH 5.0, sodium acetate; pH 5.5, MES [2-(*N*-morpholino)-ethane sulfonic acid]; pH 6.0, MES; pH 6.5, MES; pH 7.0, MOPS [3-(*N*-Morpholino)-propanesulfonic acid]; pH 7.5, MOPS; pH 8.0, 10 mM Tris [Tris (hydroxymethyl) aminomethane]; pH 8.5, 10 mM Tris; pH 9.0, 10 mM Tris. For voltammetry, OmcA with lipid-binding site and a tetracysteine tag was exchanged into 10 mM MOPS buffer (pH 7) with 10 mM KCl using Microcon YM-10 spin columns. Because these solutions were not diluted, the protein concentration was about 2.3 times higher for voltammetry than for OWLS.

2.3. Electrochemistry

2.3.1. Iron oxide and ITO electrodes

We used natural hematite (α-Fe_2O_3) single crystals as electrodes; they are n-type, with donor impurities of Ti, along with significant Sn and V, totaling about 2×10^{-3} atomic percent as indicated by laser ablation ICP-MS (these electrodes have been characterized previously [43]). Indium–tin oxide (ITO; 90% In_2O_3, 10% SnO_2) films deposited on quartz substrates were obtained from Delta Technologies, Limited, Stillwater, MN, USA and cut into 4×10 mm pieces for use as electrodes.

2.3.2. Electrochemical configuration

Cyclic voltammetry was conducted using a Molecular Imaging Picostat (Molecular Imaging, Tempe, Arizona, USA). Clean hematite crystals (thin plates) were glued to substrates using silver paste and masked with silicone rubber to leave about 1 cm^2 of the (0 0 1) crystal face exposed. In the shorter-term experiments, we used a Teflon well to hold four drops of OmcA solution and dipped the hematite working electrode into the solution along with a Pt counter electrode and an Ag/AgCl reference electrode. For longer-term experiments, two drops of OmcA solution were placed on the exposed face, and the counter and reference electrodes inserted into the drops. Because of the very small volume, we used a Pt wire counter electrode, an oxidized Ag wire quasi-reference electrode which was calibrated against an Ag/AgCl reference electrode and found to be about 60 mV negative of Ag/AgCl. Both assemblies were enclosed in a container connected to a flowing water-saturated N_2 gas source during analysis. For the longer-term experiment, the solution was allowed to sit on the electrode at 4 °C overnight in a closed container in air, allowing for adsorption of protein to the electrode surface and for oxidation of the hemes. Scans started at 0.6 V after a 5 s conditioning period, scanned to −0.6 or −0.8 V (see figures), and returned to 0.6 V (some points were lost at the end of scans because of manual scan termination to avoid data overwrite), with the exception of two scans that were started at 0.3 V (Fig. 6c) to see if this affected the outcome (it did not). Scan speed was 50 mV s^{-1} in all cases.

Differential pulse voltammograms were taken using a CH Instruments (CHI, Austin, Texas, USA) potentiostat with a 0.004 V increment, 0.05 V pulse amplitude and 0.025 s pulse width, sampling for 0.0083 s after pulse, and a 0.2 s pulse period.

2.4. Atomic force microscopy (AFM)

AFM imaging was accomplished using a Digital Instruments Nanoscope IIIa Multimode AFM (Veeco Instruments, Woodbury, NY, USA) operated in contact mode (in order to vary tip-surface contact forces) using a fluid cell. Cleaned (0 0 1) faces of hematite single crystals (see Section 2.3.1) were used.

3. Results and discussion

3.1. OWLS/AFM

OWLS results for the adsorption of OmcA to Al_2O_3 are shown in Fig. 1. Although initial adsorption is rapid, slow adsorption continues for up to 45 min (e.g., pH 8). When the post-adsorption change in signal was similar to the pre-adsorption drift in the baseline, we deemed the adsorption phase to be complete within our ability to detect it and initiated the desorption phase by injecting protein-free buffer (same concentration and pH). Desorption upon dilution is minimal in all cases except at high pH, where slow desorption is observed.

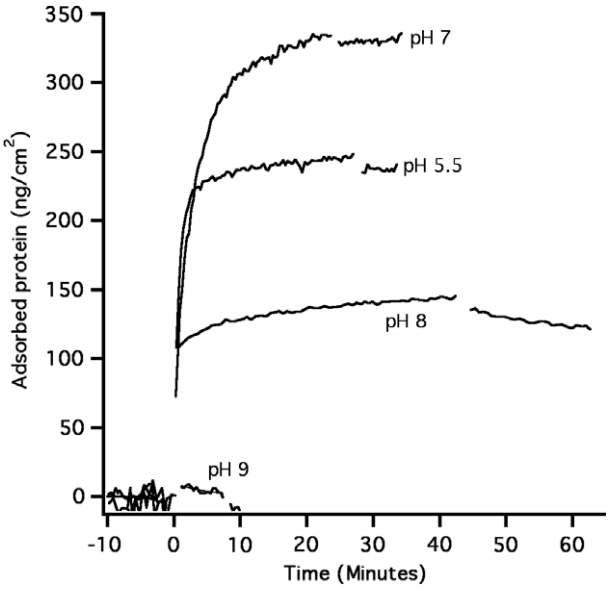

Fig. 1. OmcA adsorption to Al_2O_3 with time (from OWLS).

Because both the transverse magnetic and transverse electric waveguide modes are measured in OWLS, two equations can be solved for the thickness (d_A) and refractive index of the adsorbed layer. However, although OWLS-determined adsorbed mass is reliable, d_A is unreliable because it can covary with layer refractive index. AFM provides an independent comparison. At pH 7, OWLS d_A had peaked at 9.3 ± 3.3 (2s) nm about 16 minutes after adsorption started, and by the end of the experiment 30 minutes later had contracted to 5.8 ± 1.0 (2s) nm (data not shown). This contracting trend is may be an artifact of submonolayer coverage in the adsorbed layer (which is consistent with coverage results described below). The final d_A may, however, be compared with AFM observations at pH 7; an OmcA solution was prepared as described above, with approximately the same concentration (based on optical density at 400 nm), and injected into the AFM. After about an hour, during which a layer of adsorbed protein formed, high contact force (~200 nN) was used to "scrape" an area of the α-Fe_2O_3 (0 0 1) surface free of adsorbed protein. Fig. 2 shows the resulting scan field, imaged at low contact force (~2 nN). The curved features correspond to single-layer steps on the relatively flat hematite surface. Drift caused the apparent distortion in the nominally square scan field. The depth of the scan field corresponds to the thickness of the adsorbed protein layer, and is on the order of 4.8 ± 2 (2s) nm in Fig. 2. This corresponds, within substantial error, with the OWLS d_A result. The AFM layer thickness is complicated by noise and the likely presence of re-sorbed OmcA molecules in the "scraped" area, leading to artificial reduction of the overall average height difference between the "clean" area and the areas more densely coated with protein.

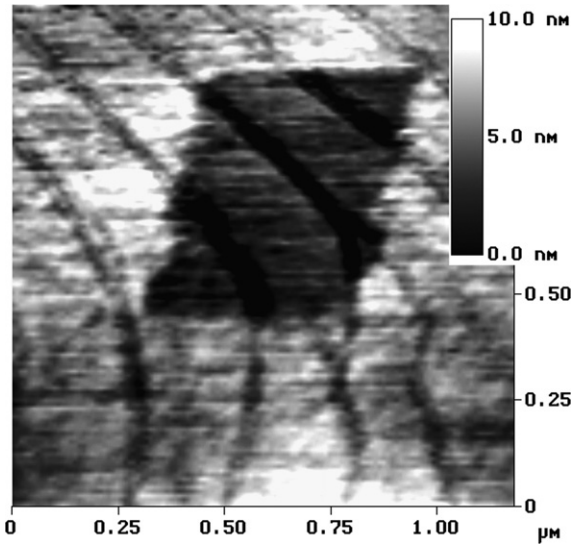

Fig. 2. Atomic force microscope (AFM) image of an OmcA layer in situ in pH 7 MOPS (see text). The image scale is in μm, and the vertical scale is in nm. The roughly parallelogram-shaped depression is a nominally square scan-field "dug" out of the protein layer by a previous scan at high contact force (see text) and distorted by drift. The average depth of this scan field is taken as an indication of the thickness of the adsorbed OmcA layer, with caveats as discussed in the text.

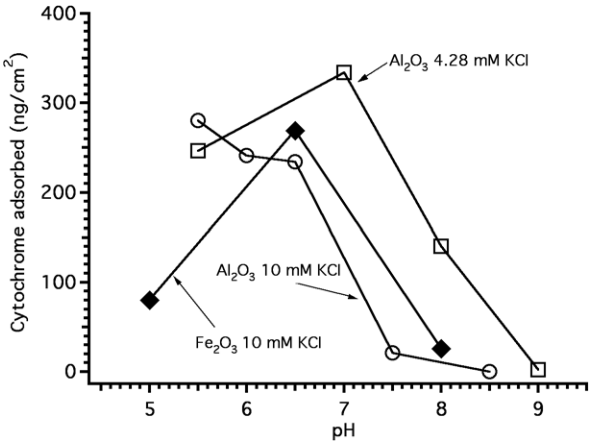

Fig. 3. OWLS results for OmcA adsorption as a function of pH for different surfaces (Al_2O_3 and Fe_2O_3) and two different KCl concentrations. Only one measurement was made at each pH value. Reproducibility in replicates using a different protein (see text) was ± 3 ng cm^{-2} (2σ), which is within the size of the symbols in this figure.

An adsorption density of 334 ng cm^{-2} (Fig. 1) corresponds to 2.4×10^{12} molecules cm^{-2} and can be explained by a monolayer of hexagonally close-packed spherical molecules of 9.9 nm in diameter (or less than a monolayer of smaller molecules). The OWLS and AFM results suggest that adsorbed OmcA molecules are somewhat thinner than this (or, again, that there is an incomplete monolayer). Alternatively, the adsorbed OmcA molecules may be roughly lens-shaped rather than spherical, with a bigger lateral footprint than the layer thickness suggests under a spherical molecule assumption. Such vertical compression and slight spreading could be caused by adsorption; the adsorptive forces may be sufficient to distort molecule shape. By comparison, Xiong et al. [27] reported a hydrodynamic radius of 9 nm, which is considerably larger as a diameter than our OWLS and AFM results at pH 7. Our results imply that the coverage is less than one monolayer at other pH values and at higher KCl concentrations.

Fig. 3 shows the pH dependence of OmcA adsorption to Al_2O_3-coated waveguides in 4.28 mM KCl and in 10 mM KCl, as well as to Fe_2O_3 in 10 mM KCl. In general, there is less adsorption in 10 mM KCl than in 4.28 mM KCl (Al_2O_3 data). This is consistent with expectation; for example, Gaspard et al. [24] showed that outer-membrane cytochromes can be solubilized from *Geobacter sulfurreducens* in a 0.5 M KCl wash. Similar techniques have been refined for other cytochromes and proteins (Tom DiChristina, pers. comm.). If OmcA is more soluble at higher ionic-strength it is reasonable to suppose, as a qualitative argument, that the amount adsorbed would decrease with increasing salt concentration as observed in our OWLS results. Peak OmcA adsorption occurs at pH 6.5–7.0 which is near the isoelectric point of OmcA (6.23; Ming Tien, pers. comm.). There appears to be a difference in adsorption at low pH between Al_2O_3 and Fe_2O_3. We speculate that OmcA begins to unfold under intramolecular charge buildup at $pH < pH_{iep}$, possibly exposing hydrophobic parts of the molecule that enhance hydrophobic expulsion from the solution and lead to greater adsorption. OmcA adsorbed to Fe_2O_3 does not, however, follow this trend. In adsorption of mitochondrial cytochrome *c* to Fe_2O_3, for example, we have observed that under relatively extreme pH conditions adsorbed cytochrome molecules can be stabilized against unfolding by association with an oxide surface [44]. Hematite may play a similar role for OmcA, to an extent greater than on Al_2O_3, leading to less adsorption (by hydrophobic expulsion of unfolded molecules from low pH solution) at low pH on Fe_2O_3 as compared with Al_2O_3. Interpolation of the Fe_2O_3 adsorption trend to pH 7.5 gives an OmcA adsorption density of approximately 100 ng/cm^2, which corresponds to 1.2 nmol/cm^2. This compares to 2.6 nmol/cm^2 reported by Xiong et al. [27] for adsorptive saturation on hematite nanoparticles. Xiong et al. [27] used 1 μM OmcA, while we used 0.58 μM OmcA, so a factor-of-two difference is within expectation. The adsorption densities observed in this study are thus entirely comparable with those of Xiong et al. within uncertainty and interpolation error; however, Xiong et al. also state that OmcA binding is specific to hematite and that OmcA does not bind to diaspore (AlOOH) or goethite (FeOOH). We find that OmcA binds in comparable amounts on both Al_2O_3 and Fe_2O_3 under the same pH and ionic strength conditions. Our reading of the Xiong et al. OmcA binding data suggests that the apparent preferential binding to hematite (Fe_2O_3) is an artifact of the mineral particle sizes used; OmcA binding to nanohematite (96 m^2 g^{-1}) is compared to binding on FeOOH and AlOOH minerals that pass a 45 μm sieve after crushing (probably <1 m^2 g^{-1}). There is probably at least a

factor of 10^2 difference in specific surface area between the nanohematite and the FeOOH and AlOOH, which would easily account for the difference in OmcA binding to Fe_2O_3 versus FeOOH and AlOOH presented in units of nanomoles adsorbed per mg sorbent. We therefore suggest that our adsorption data and those of Xiong et al. [27] are in agreement and that OmcA, in fact, binds in similar quantities to Fe and Al oxides when normalized to surface area.

Exponential fits were made to the OWLS adsorption data, and first-order rate constants are plotted in Fig. 4. The rate of OmcA adsorption to Al_2O_3 tends to be higher at low pH (suggesting a different mechanism from that operating at pH 7), although the pH 8 point for the 4.28 mM KCl case gave a large rate constant at high pH as well. At low pH, especially with the positive surface charge of Al_2O_3 increasing to a maximum at roughly pH 5 [45], electrostatic repulsion between the protein and the surface should be significant. The substantial adsorption observed at this pH suggests that chemical bonding or hydrophobic interactions become important at low pH. The pH 8 time series was better described by a double exponential, with two distinct rate constants (4.38 min^{-1}, 0.0654 min^{-1}). The reasons for this are unknown, but additional investigations of the pH-dependence of adsorption rate are being undertaken. In contrast to the Al_2O_3 results, the adsorption of OmcA on Fe_2O_3 takes place at a fairly uniform rate over the pH range, with slightly higher rates at low pH. If, as with alumina, the adsorption rate is higher near the pH at which maximum positive surface charge is reached, then the adsorption rate should increase as pH is decreased to about 3 for hematite. At such low pH, however, intramolecular positive charge would likely unfold the OmcA molecule to a much greater extent than at pH 5.

3.2. Cyclic voltammetry

Compared to controls run in 10 mM KCl (Fig. 5a), voltammograms with pH 7 OmcA solution (prepared as described above in reduced form) exhibited greater capacitive hysteresis, probably due to a change in the nature and charge of molecules in the vicinity of the electrode surface. We have not attempted to interpret this effect in detail. In addition, they revealed a very small cathodic peak at −370 mV due to reduction of small amounts of oxidized protein that were created, most probably, during an initial 5 s settling time at the starting potential of +600 mV. There is a broad anodic peak centered at about −50 mV, suggesting a midpoint potential of about −210 mV versus Ag/AgCl (Table 1).

In contrast, after an overnight incubation at 4 °C, during which time OmcA adsorbed to the hematite electrode

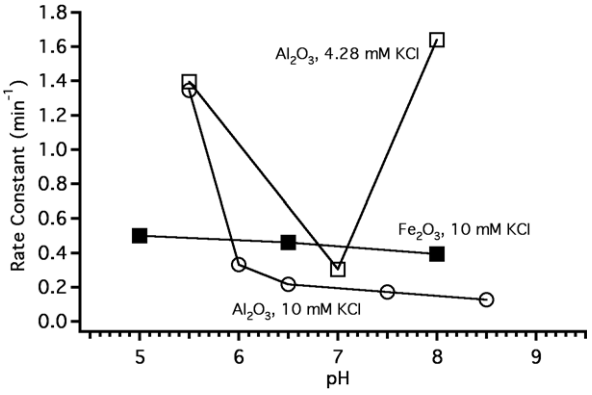

Fig. 4. First-order adsorption rate constants obtained by fitting the OWLS data (for examples, see Fig. 1) with an exponential function.

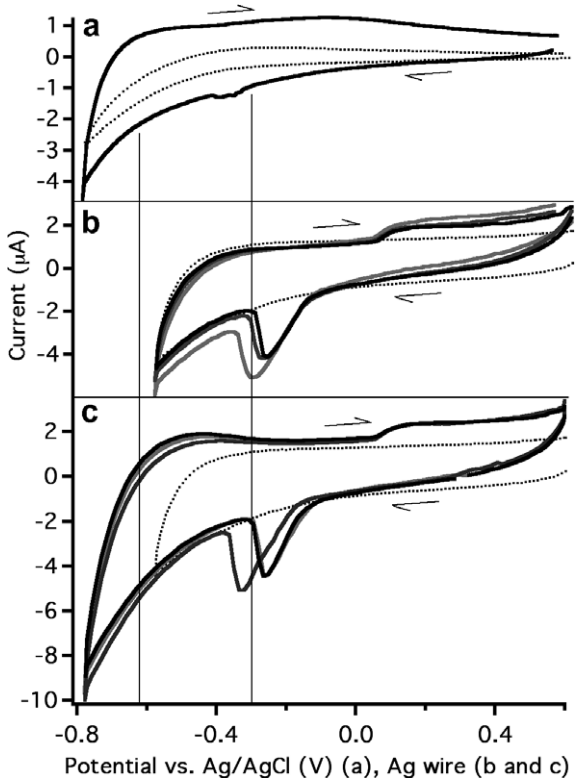

Fig. 5. Voltammograms of OmcA taken under different conditions using Fe_2O_3 electrodes. All scans taken at 50 mV s^{-1}. Arrows give the scan direction, the vertical line at −0.3 V gives the approximate flatband potential of Fe_2O_3, and the vertical line at −0.62 V gives the approximate H^+ reduction potential. (a) Control scan (10 mM KCl; dotted) for the same electrode used to take a voltammogram of the OmcA-containing solution (solid); scans used an Ag/AgCl reference. (b) Control scan (10 mM KCl; dotted) for the Fe_2O_3 electrode used in the overnight incubation (see text) taken prior to exposure to protein. Three voltammograms were taken in succession, in the order of increasingly dark solid lines. (c) the same control scan from (b), with three scans taken in succession to −800 mV, again in the order of increasingly dark lines. (b) and (c) used an Ag wire quasi reference (see text).

Table 1
Cathodic, anodic and midpoint potentials (volts vs. Ag/AgCl) from Fig. 5

	$E_{cathodic}$ (V)	E_{anodic} (V)	$E_{midpoint}$ (V)
Solution	−0.37	−0.05	−0.21
Adsorbed	−0.38 to −0.32	+0.06	−0.16 to −0.13

surface and was oxidized, because it was stored in air and exposed to oxygen, the three voltammograms in Fig. 5b exhibit a far more pronounced cathodic peak (electrons flowing from the electrode to the hemes in the protein) at potentials ranging from −260 to −320 mV, and a smaller but also more pronounced anodic peak at about +120 mV. These correspond to −380 to −320 mV and +60 mV vs. Ag/AgCl after correction for the Ag wire with midpoint potentials of −160 to −130 mV vs. Ag/AgCl. The apparent midpoint potential for protein in solution (though some protein had likely adsorbed in the time between injection of solution and obtaining the voltammogram) is thus more negative than that of the adsorbed protein. We speculate that the protein conformation changes upon adsorption, so as to change the potentials of the hemes. Xiong et al. [27] note a decrease in solvent accessibility of tryptophans in OmcA upon OmcA binding to hematite nanoparticles. If such changes in solvent accessibility extend to the hemes in OmcA, this would most likely affect their redox potential [46,47].

We measured the flatband potential (V_{FB}) of the natural hematite crystals using a method described previously [48] and found it to be −0.3 V ± 0.1 V at pH 7. Thus, the cathodic peak occurs in a potential region very close to the flatband potential of the electrode, and no Schottky barrier to electron transfer should exist. The anodic peaks, however, are 300–450 mV positive of V_{FB}, and a Schottky barrier should exist. This helps explain why current flows more readily to the protein from the electrode than back from the electrode to the protein (rectification).

For the incubated electrode, we scanned first to −600 mV (Fig. 5b), and then scanned to −800 mV (Fig. 5c) in order to check for any unusually negative-potential peaks. It is striking that there is variation in the position and width of the cathodic peak from scan to scan (Fig. 5b and c), but no variation in the position of the anodic peak. In Fig. 5b and c, the scans were taken in order of increasingly dark lines. The first scan to −600 mV (Fig. 5b) is broad; subsequent scans are narrower with a less negative cathodic peak. When scanning to −800 mV (Fig. 5c), only the middle scan was wider and more negative.

Field et al. [22] have characterized an OmcA homolog from *Shewanella frigidimarina*, and shown that the 10 hemes are reduced at −243 and −324 mV versus SHE (corresponding to about −443 and −524 versus Ag/AgCl). We may be reducing hemes in OmcA from *S. oneidensis* MR-1 at two or more different potentials (Fig. 5b and c) as well. There are many possible explanations for these observations, including intramolecular electron hopping between hemes (perhaps coupled to conformational changes) as well as potential-induced changes in OmcA molecular orientation on the surface, that may affect the current to particular hemes at particular potentials from scan to scan in Fig. 5b and c. At present, we can only speculate about which combination of such effects may give rise to our observations. In this context, it is also interesting that after the six scans presented in Fig. 5 for adsorbed protein, the 7th scan was completely different (Fig. 6). In this 7th scan, the cathodic peaks seen in Fig. 5 are no longer present, and only two much smaller cathodic peaks are observed at very negative potential. The oxidation (anodic) peak is also absent, indicating that we cannot have reduced H^+ to H_2 during the scans to −800 mV (Fig. 5c) in amounts sufficient to reduce OmcA and prevent cathodic current; if OmcA had been reduced by H_2, we would still expect to see an oxidation peak. It is possible that the OmcA desorbed, but the OWLS results suggest that OmcA should not desorb in the reduced state. Though this question bears further study, we speculate that the loss of redox peaks reflects either a substantial conformation or orientation change on the part of the adsorbed protein such that previously available redox sites (presumably hemes) are no longer able to accept electrons and only a redox site with a much more negative potential is available. In a biofuel cell application, we would not expect to bring the anode to −800 mV and would in general not expect to cause cathodic current but rather to maintain the anode at a sufficiently oxidizing potential to maintain anodic current. The cyclic voltammetry experiments should thus not be taken as an indication of OmcA instability in a biofuel cell. Indeed, it may be quite useful if the adsorbed enzyme in a biofuel cell acts as a diode, preventing "backwards" current flow.

For OmcA from *S. oneidensis* MR-1, others have observed cathodic peak potentials similar to those we report here using metal electrodes (David Richardson, pers. comm.).

Within uncertainty in the electrode area, the amount of current that flows in the widest of the cathodic peaks in Fig. 5 is about the same as that needed to reduce all the hemes in an OmcA monolayer as measured by OWLS (equivalent to 2.75×10^{12} molecules cm^{-2} as compared to 2.4×10^{12} molecules cm^{-2} from OWLS). Because the concentration of protein was about 2.3 times higher for the voltammetry experiments than that in the OWLS experiments, it would not be surprising if more protein had adsorbed for the electrochemical experiments. In addition,

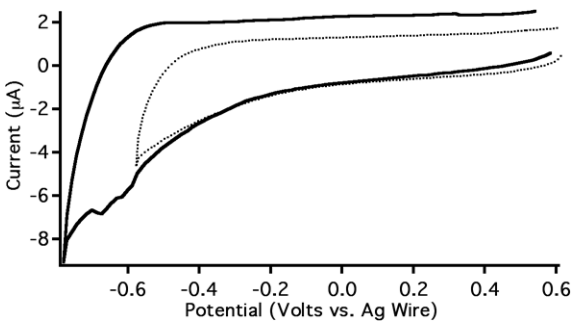

Fig. 6. The voltammogram (solid; 50 mV s^{-1}) recorded immediately after those in Fig. 5, with the same control scan (dotted) for comparison. The large cathodic peaks at −320 to −380 mV (vs. Ag wire quasi reference) are absent, and new smaller cathodic peaks occur at more negative potential.

there was OmcA remaining in solution that could accept electrons from reduced OmcA on the surface; residual oxygen might also play a role. In any case, it is likely that in these electrochemical experiments, we are reducing and oxidizing most or all of the available hemes in the adsorbed protein. Why, after six scans, it was no longer possible to substantially reduce or oxidize the OmcA (note the absence of an anodic peak in Fig. 6) is not known.

We may speculate that OmcA, having the biochemical role of reductant for iron oxide, may undergo a conformation change, a re-orientation on the surface, or possibly desorb rather than be reduced by iron oxide. We also note that, in nature, OmcA does not operate in isolation. OmcA is known to complex with another outer-membrane decaheme cytochrome, MtrC, in a 2:1 OmcA:MtrC ratio [42]. The complex may operate in a completely different manner than does isolated OmcA. For example, a complete catalytic cycle, with electron transfer to iron oxide followed by "reloading" with electrons from upstream in the electron transport chain, may require a complete complex as well as other as yet unknown proteins or other molecules. The approach to optimal use of these cytochromes in a biofuel cell application will depend on better understanding these many interactions, and the present study is simply an initial step in this direction.

3.3. Differential pulse voltammetry

We compared voltammetry of OmcA solution interacting with hematite to that of OmcA solution interacting with ITO. Because hematite and ITO electrodes exhibit different capacitive hysteresis in voltammetry, we used differential pulse voltammetry for the comparison (Fig. 7). OmcA solution interacting with the ITO electrode gave far higher currents than did OmcA solution interaction with hematite. The voltammogram with the hematite electrode contains small peaks at −300 mV and +80 mV, but are not visible in Fig. 7 in comparison to the much larger peaks at −90 mV and −410 mV in the voltammogram with ITO. The origin of the less negative of these peaks in the differential pulse voltammetry is not known, but the peaks at −300 to −410 mV are consistent with observations made above using linear sweep voltammetry. Although further work is warranted, these initial results suggest that hematite is not the only electrode with which OmcA will interact and that hematite may not be the best electrode material for an OmcA-based biofuel cell application. The V_{FB} for ITO is about the same as that of hematite [49], so there should be little difference in the height of the Schottky barrier for these two materials at a given potential. The dopant concentration is much higher for ITO ($\sim 10^{21}$ cm^{-3}) than for the natural hematite electrodes ($\sim 10^{17}$ cm^{-3}), however, so the thickness of the space charge layer should be much greater for hematite than for ITO and the charge carrier concentration near the electrode surface is much higher for ITO than for hematite.

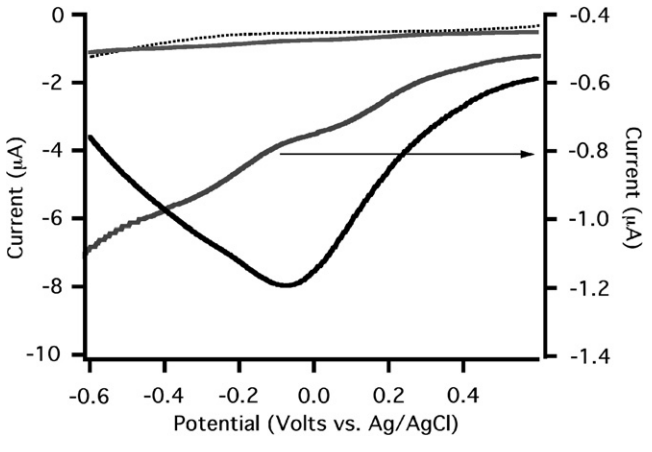

Fig. 7. Differential pulse voltammetry of OmcA solutions using Fe_2O_3 (gray lines) and ITO (solid) electrodes. Control scans with KCl and buffer are very similar and given by the dotted line (there may have been residual oxygen present in the system, leading to slightly higher current at the lowest potentials). The voltammogram using an Fe_2O_3 electrode is plotted twice, once with a vertical scale expanded by a factor of 10 (horizontal arrow indicates which voltammogram goes with the right-hand scale).

The hematite conduction band edge has somewhat higher energy than that of ferric hydroxides [50], which would make any Schottky barrier easier to surmount for such materials as goethite and lepidocrocite (polymorphs of FeOOH) than for hematite. These and other hydroxide minerals are more common in nature than hematite, so we speculate that the midpoint potentials of the OmcA are optimized for reduction of these minerals and that hematite is probably not the optimum electron acceptor in natural reduction of ferric iron by dissimilatory iron reducing bacteria.

4. Conclusions

The 85 kDa *c*-type decaheme cytochrome OmcA has characteristics that are of interest in microbial- and biofuel cells, including the ability to adsorb to and remain catalytically active on oxide and other solid surfaces [27]. Here, we show that OmcA adsorbs over a range of pH values and that its adsorptive binding is not restricted to hematite but extends to other oxide materials as well. The diameter of adsorbed OmcA at pH 7 varies from 4.8 ± 2 nm from AFM layer thickness to 5.8 ± 1.1 nm from OWLS measurements and up to 9.9 nm from spherical packing arguments. We demonstrate direct electrochemistry between hematite and ITO electrodes; electron transfer between iron oxide and OmcA occurs with an electron flux of over 10^{13} electrons cm^{-2} s^{-1}, in rough agreement with the results of Xiong et al. [27]. Finally, we show that electrode area-normalized current between OmcA and a hematite electrode is substantially lower than between OmcA and an ITO electrode, suggesting that materials such as ITO, metallic conductors, or woven graphite fibers may make better electrodes in microbial fuel cells.

Acknowledgements

A portion of this research was performed as part of an EMSL Biogeochemistry Grand Challenge project (Eggleston, Shi, Lower, Droubay) at the W.R. Wiley Environmental Molecular Sciences Laboratory, a national scientific user facility sponsored by the US Department of Energy's Office of Biological and Environmental Research and located at Pacific Northwest National Laboratory. PNNL is operated for the Department of Energy by Battelle. Eggleston and Colberg acknowledge the support of the US National Science Foundation (EAR0434019) and the US Department of Energy (DOE42607); the contents of this paper represent the views of the authors and not of the above-named agencies.

References

[1] M. Vargas, K. Kashefi, E.L. Blunt-Harris, D.R. Lovley, Nature 395 (1998) 65.
[2] B.L. Beard, C.M. Johnson, L. Cox, H. Sun, K.H. Nealson, C. Aquilar, Science 285 (1999) 1889.
[3] D.R. Lovley, Microbiol. Rev. 55 (1991) 259.
[4] D.R. Lovley, E.F. Phillips, D.J. Lonergan, Environ. Sci. Technol. 25 (1991) 1062.
[5] D.R. Lovley, E.J.P. Phillips, Appl. Environ. Microbiol. 54 (1988) 1472.
[6] J.M. Myers, K.H. Nealson, Science 240 (1988) 1319.
[7] K.H. Nealson, D. Saffarini, Ann. Rev. Microbiol. 48 (1994) 311.
[8] D.R. Lovley, Adv. Agron. 54 (1995) 175.
[9] J.D. Coates, E.J. Phillips, D.J. Lonergan, H. Jenter, D.R. Lovley, Appl. Environ. Microbiol. 62 (1996) 1531.
[10] T.L. Kieft, J.K. Frederickson, T.C. Onstott, Y.A. Gorby, H.M. Kostandarithes, T.J. Bailey, D.W. Kennedy, S.W. Li, A.E. Plymale, C.M. Spandoni, M.S. Gray, Appl. Environ. Microbiol. 65 (1999) 1214.
[11] K. Kashefi, D.E. Holmes, A.-L. Reysenback, D.R. Lovley, Appl. Environ. Microbiol. 68 (2002) 1735.
[12] K. Kashefi, D.E. Holmes, J. A Baross, D.R. Lovley, Appl. Environ. Microbiol. 69 (2003) 2985.
[13] D.E. Cummings, O.L. Snoeyenbos-West, D.T. Newby, A.M. Niggemyer, D.R. Lovley, M.J. Achenbach, R.F. Rosenzweig, Microbial Ecol. 46 (2003) 257.
[14] S.E. Childers, A. Ciufo, D.R. Lovley, Nature 416 (2002) 767.
[15] D.R. Lovley, J.D. Coates, E.L. Blunt-Harris, E.J.P. Phillips, J.C. Woodward, Nature 382 (1996) 445.
[16] G. Reguera, K.D. McCarthy, T. Mehta, J.S. Nicoll, M.T. Tuominen, D.R. Lovley, Nature 435 (2005) 1098.
[17] Y.A. Gorby, S. Yanina, J.S. McLean, K.M. Rosso, D. Moyles, A. Dohnalkova, T.J. Beveridge, I.S. Chang, B.H. Kim, K.S. Kim, D.E. Culley, S.B. Reed, M.F. Romine, D. Saffarini, E.A. Hill, L. Shi, D.A. Elias, D.W. Kennedy, G. Pinchuk, K. Watanabe, S. Ishii, B. Logan, K.H. Nealson, J.K. Frederickson, Proc. Natl. Acad. Sci. 103 (30) (2006) 11358.
[18] J.F. Heidelberg, I.T. Paulsen, K.E. Nelson, E.J. Gaidos, W.C. Nelson, T.D. Read, J.A. Eisen, R. Seshadri, N. Ward, B. Methe, R.A. Clayton, T. Meyer, A. Tsapin, J. Scott, M. Beanan, L. Brinkac, S. Daugherty, R.T. Deboy, R.J. Dodson, A.S. Durkin, D.H. Haft, J.F. Kolonay, R. Madupu, J.D. Peterson, L.A. Umayam, O. White, A.M. Wolf, J. Vamathevan, J. Weidman, M. Impraim, K. Lee, K. Berry, C. Lee, J. Mueller, H. Kouri, J. Gill, T.R. Utterback, L. A McDonald, T.V. Feldblyum, H.O. Smith, J.C. Venter, K.H. Nealson, C.M. Fraser, Nat. Biotechnol. 20 (2002) 1118.
[19] B.A. Methe, J. Webster, K. Nevin, J.A. Eisen, I.T. Paulsen, W. Nelson, J.F. Heidelberg, D. Wu, M. Wu, N. Ward, M.J. Beanan, R.J. Dodson, R. Madupu, L.M. Brinkac, S.C. Daugherty, R.T. Deboy, A.S. Durkin, M. Gwinn, J.F. Kolonay, S.A. Sullivan, D.H. Haft, J. Selengut, T.M. Davidsen, N. Zafar, O. White, B. Tran, C. Romero, H.A. Forberger, J. Weidman, H. Khouri, T.V. Feldblyum, T.R. Utterback, S.E. Van Aken, D.R. Lovley, C.M. Fraser, Science 302 (2003) 1967.
[20] Y.A. Gorby, D.R. Lovley, Appl. Environ. Microbiol. 57 (1991) 867.
[21] A.S. Beliaev, D. Saffarini, J. Bacteriol. 180 (1998) 6292.
[22] S.J. Field, P.S. Dobbin, M.R. Cheesman, N.J. Watmough, A.J. Thomson, D.J. Richardson, J. Biol. Chem. 275 (2000) 8515.
[23] C.R. Myers, J.M. Myers, Lett. Appl. Microbiol. 37 (2003) 254.
[24] S. Gaspard, F. Vazquez, C. Holliger, Appl. Environ. Microbiol. 64 (1998) 3188.
[25] S. Seeliger, R. Cord-Ruwisch, B. Schink, J. Bacteriol. 180 (1998) 3686.
[26] T.S. Magnuson, N. Isoyama, A.L. Hodges-Myerson, G. Davidson, M.J. Maroney, G.G. Geesey, D.R. Lovley, Biochem. J. 359 (2001) 147.
[27] Y. Xiong, L. Shi, B. Chen, M.U. Mayer, B.H. Lower, Y. Londer, S. Bose, M.F. Hochella Jr., J.K. Frederickson, T.C. Squier, J. Am. Chem. Soc. 128 (2006) 13978.
[28] B.E. Logan, B. Hamelers, R. Rozendal, U. Schroeder, J. Keller, S. Freguia, P. Aeltermann, W. Verstraete, K. Rabaey, Environ. Sci. Technol. 40 (2006) 5181.
[29] D.R. Lovley, Curr. Opin. Biotechnol. 17 (2006) 327.
[30] K.M. Rosso, D.M.A. Smith, M. Dupuis, J. Chem. Phys. 118 (2003) 6455.
[31] A. Kay, I. Cesar, M. Graetzel, J. Am. Chem. Soc. 128 (2006) 15714.
[32] W. Lukosz, Sensor. Actuat. B 29 (1995) 37.
[33] P.G. Kurrat, M. Textor, J.J. Ramsden, P. Boeni, N.D. Spencer, Rev. Sci. Instrum. 68 (1997) 2172.
[34] C. Calonder, Y. Tie, P.R. Van Tassel, Proc. Natl. Acad. Sci. 98 (2001) 10664.
[35] F. Höök, J. Vörös, M. Rodahl, R. Kurrat, P. Boni, J.J. Ramsden, M. Textor, N.D. Spencer, P. Tengvall, J. Gold, B. Kasemo, Colloid. Surf. B 24 (2002) 155.
[36] Y. Tie, C. Calonder, P.R. Van Tassel, J. Colloid. Interf. Sci. 268 (2003) 1.
[37] J. Vörös, Biophys. J. 87 (2004) 553.
[38] J. Vörös, J.J. Ramsden, G. Csucs, I. Szendro, S.M. De Paul, M. Textor, N.D. Spencer, Biomaterials 23 (2002) 3699.
[39] Y.J. Kim, Y. Gao, S.A. Chambers, Surf. Sci. 371 (1997) 358.
[40] T.C. Droubay, S.M. Heald, K.M. Rosso, D.E. McCready, S.A. Chambers, C.M. Wang, Phys. Rev. B. 75 (2007) 104412.
[41] L. Shi, L. Jiann-Trzwo, L.M. Markillie, T.C. Squier, B.S. Hooker, BioTechniques 38 (2005) 297.
[42] L. Shi, B. Chen, Z. Wang, D.A. Elias, M.U. Mayer, Y.A. Gorby, S. Ni, B.H. Lower, D.W. Kennedy, D.S. Wunschel, H.M. Mottaz, M.J. Marshall, E.A. Hill, A.S. Beliaev, J.M. Zachara, J.K. Frederickson, T.C. Squier, J. Bacteriol. 188 (2006) 4705.
[43] C.M. Eggleston, A.G. Stack, K.M. Rosso, S.R. Higgins, A.M. Bice, S.W. Boese, R.D. Pribyl, J.J. Nichols, Geochim. Cosmochim. Acta 67 (2003) 985.
[44] N. Khare, C.M. Eggleston, D.M. Lovelace, S.W. Boese, J. Colloid. Interf. Sci. 303 (2006) 404.
[45] W. Stumm, J.J. Morgan, Aquatic Chemistry, third ed., Wiley, New York, 1996, p. 1022.
[46] T.J.T. Pinheiro, Biochimie 76 (1994) 489.
[47] F.A. Tezcan, J.R. Winkler, H.B. Gray, J. Am. Chem. Soc. 120 (1998) 13383.
[48] G. Boschloo, D. Fitzmaurice, J. Phys. Chem. B 103 (1999) 3093.
[49] J.E.A.M. van den Meerakker, E.A. Meulenkamp, M. Scholten, J. Appl. Phys. 74 (1993) 3282.
[50] J.K. Leland, A.J. Bard, J. Phys. Chem. 91 (1987) 5076.